Enhanced Micro-Doppler Feature Analysis for Drone Detection

Yimin D. Zhang [*], Xingyu Xiang [#], Yi Li [#], and Genshe Chen [#]

[*] Department of Electrical and Computer Engineering, Temple University, Philadelphia, PA
[#] Intelligent Fusion Technology, Inc., Germantown, MD

Abstract

As low-cost drones become more accessible, they pose various safety, security, and privacy threats. As such, it becomes increasingly important to detect their presence, locate and track their positions, and classify their types in real time. In this paper, we perform time-frequency analyses of drone Doppler and micro-Doppler signatures to provide enhanced drone detection and feature extraction capabilities. The analyses are based on the combined use of spectrogram and inverse Radon transform (IRT). The paired property of propeller blades associated with a rotor is further utilized to compute the IRT product for enhanced performance. It is demonstrated that the IRT and IRT product images, when expressed in terms of the rotation frequency and blade position phase, provide flexibility and effectiveness for the presentation and estimation of these parameters.

1. Introduction

Drones, or small unmanned aerial vehicles (UAVs), are becoming more accessible and render increasing penetration into our daily life. While they have brought significant capabilities and potentials in enabling and enhancing surveillance and communication capabilities and have found broad applications in various commercial, homeland security, and military applications [1, 2], they also pose great challenges in detecting and preventing drones from unauthorized intrusions. As such, it becomes an emergent task to detect and classify drones in a scene with the presence of other targets and clutter.

Drone Doppler signatures, particularly the micro-Doppler signatures due to fast blade rotations, are considered important for drone detection and classifications [3-5]. The micro-Doppler signatures, when properly processed, reveal the number of rotors and blades, their rotation rates, and blade length [6, 7]. Time-frequency (TF) analyses are effective to analyze time-varying Doppler and micro-Doppler signatures [8, 9]. The short-time Fourier transform (STFT) is a commonly used TF analysis methods due to its simplicity and robustness [3-5]. The magnitude square of STFT is referred to as the spectrogram. Alternative TF analysis methods are based on bilinear TF distributions with proper kernels or exploiting compressive sensing techniques [9-13].

While TF analysis of rotating blades have been extensively considered for helicopters, the micro-Doppler signatures of drones are much more challenging to analyze because of the equipment of multiple rotors and more propeller blades. In particular, as drones have multiple rotors which generally rotate in different frequencies and phases, the time-varying micro-Doppler signatures become complicated. As a result, the spectrogram, or an alternative TF distribution, does not provide a clear representation of such micro-Doppler signatures for analysis and parameter estimation. The TF signature analysis and recognition become even more challenging when the input signal-to-noise ratio (SNR) is low.

On the other hand, the structure associated with the micro-Doppler signatures can be utilized to enhance their characterizations. First, due to the strong periodicity of the drone rotor rotations, the micro-Doppler signatures are characterizable with certain key parameters to enable inverse Radon transform (IRT) for enhanced feature representation and extraction of radar signals corresponding to drones. The IRT projects a sinusoidal pattern in the TF plane (TF representation of sinusoidally FM signal) to a two-dimensional (2-D) delta pulse in the IRT domain [14]. Second, most drone propellers have two or three blades that are symmetrically positioned with 180º or 120º phase differences. Such property can be used to produce IRT product for enhanced parameter estimation.

In this paper, we perform TF analyses of Drone Doppler and micro-Doppler signatures to provide enhanced drone detection and feature extraction capabilities. The analyses utilize spectrogram analysis, inverse Radon transform, and fusion of blade signatures. It is demonstrated that the IRT images, when expressed in terms of the rotation frequency and blade phase, provide flexibility and effectiveness for the presentation and estimation of these parameters. The fusion of symmetrical blade signature further enhances the signature in low SNR scenarios.

2. Signal Model

Consider a drone that exploits D rotors, each with K blades. In the example illustrated in Fig. 1, D=4 and K=2. Consider one of the rotors and denote L_1 as the distance between the blade roots and the center of the rotation, and L_2 as the distance between the blade tip and the center of the rotation. Let $\Delta L = L_2 - L_1$, and $\bar{L} = (L_1 + L_2)/2$. Then, for rotors with horizontal blade rotations as shown in Figs. 1 and 2, at a range cell where a drone is present, the slant range between the radar and the center of the kth blade of the dth rotor is given as

$$r_{d,k}(t) = R_0 + vt + H\cos(\beta)\cos(\theta_d) + \bar{L}\cos(\beta)\cos\big(\phi_{d,k}(t)\big), \quad (1)$$

where R_0 is the initial distance between the drone center with the radar, v is the radial velocity of the drone fuselage, t is the slow time, H is the distance between the rotor center to the drone center, θ_d is the rotor position angle, β is the elevation angle of the rotor to the radar line-of-sight (LOS), and $\phi_{d,k}(t) = \phi_{d,k}(0) + \omega_d t$ is the phase of the kth blade of the dth rotor, with $\phi_{d,k}(0)$ denoting the initial rotation angle, and ω_d is the rotation radian frequency of the dth rotor.

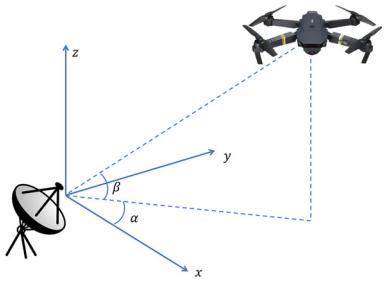

Fig. 1. Model of drone Doppler and micro-Doppler.

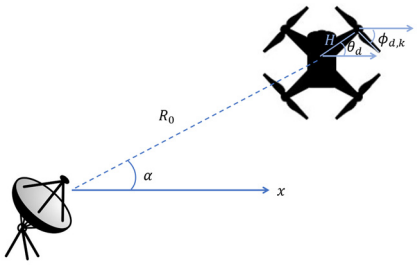

Fig. 2. Top view of the system model.

Accordingly, extending from model for helicopters [15], the slow-time data of the drone can be modeled as:

$$x(t) = \sum_{k=1}^{K} x_k(t) = A\Delta L \sum_{k=1}^{K} \text{sinc}\left[\frac{2\pi\Delta L}{\lambda}\cos(\beta)\cos(\phi_k)\right] \exp\left(-j\frac{4\pi}{\lambda}r_{d,k}\right), \quad (2)$$

where A is a scalar representing the signal strength. Considering a short coherent processing interval, the phase term $\exp\left(-j\frac{4\pi}{\lambda}r_{d,k}\right)$ is grouped into three terms,

$$\exp\left(-j\frac{4\pi}{\lambda}r_{d,k}\right) = \exp\left(-j\frac{2\pi}{\lambda}R_{0,d} - j2\pi f_D t - j\frac{4\pi}{\lambda}\tilde{r}_{d,k}\right), \quad (3)$$

where $R_{0,d} = R_0 + H\cos(\beta)\cos(\theta_d)$ is the initial position of the dth rotor and $f_D = 2v/\lambda$ is the Doppler of the drone fuselage. The last term in Eq. (3) associated with rapidly time-varying range

$$\tilde{r}_{d,k} = \bar{L}\cos(\beta)\cos\left(\phi_{d,k}(t)\right) \quad (4)$$

stands for the micro-Doppler signature with sinusoidal instantaneous frequencies.

The instantaneous micro-Doppler frequency can be obtained from Eqs. (2)-(4) as

$$\tilde{f}_{d,k} = -\frac{2}{\lambda}\bar{L}\omega_d\cos(\beta)\sin\left(\phi_{d,k}(t)\right). \quad (5)$$

3. Time-Frequency Analyses of Micro-Doppler Signatures

3.1 Short-Time Fourier Transform and Spectrogram

STFT is a commonly used representation for the classification of drone and helicopter with other objects. The STFT of a discrete-time signal $x(t)$ is given as

$$\text{STFT}(t,f) = \sum_{i=1}^{N} x(t-i)w(i)e^{-\frac{j2\pi if}{N}}, \quad (6)$$

where f is the frequency index and $w(t)$ is a window with length N. Different windows, such as the Hanning and Hamming, can be used to trade off between sidelobe levels and the mainlobe width. The window length N is a key parameter which must be properly chosen such that the yielding STFT has good resolutions in both time and frequency domains. A small value of N yields good time resolution but poor frequency resolution, and a large value of N renders a good frequency resolution but the time resolution will degrade. STFT is usually expressed in terms of its magnitude square, referred to as spectrogram.

Fig. 3 shows the spectrogram of four-blade drone signals where the input SNR is defined as the power ratio between the power of each blade to the noise power. The carrier frequency is 30 GHz, and the pulse repetition frequency is 50 kHz. The radar cross section (RCS) of the fuselage is assumed to be 20 dB higher than that of a blade. The translational motion of the drone fuselage is compensated and the direct-current (DC) component reflecting the fuselage reflection is mitigated through simple DC signal removal. As such, we only consider the micro-Doppler signatures.

Fig. 3(a) shows the spectrogram of a single-rotor case for clear visibility of the sinusoidally time-varying micro-Doppler signatures. The rotor has two blades that are separated by 180° rotating at 50 Hz (3,000 rotations per minute, rpm), rendering symmetrical micro-Doppler signatures. Fig. 3(b) shows the spectrogram when the signals corresponding to all four rotors are superimposed. The propellers rotate at 50 Hz (3,000 rpm), 55 Hz (3,300 rpm), 52 Hz (3,120 rpm), and 58 Hz (3,480 rpm), respectively. Note that, when the rotors have different rotation frequencies, their respective peak micro-Doppler frequencies differ as well. With all the eight components mixed, direct recognition of the sinusoidal patterns becomes difficult in this figure. Compared to helicopters with a single rotor [15], the micro-Doppler signature of drones are much more complicated.

In Figs. 3(c) and 3(d), we show the spectrogram of the same four-rotor drones, but with lower input SNR levels of -14 dB and -17 dB, respectively. As the input SNR reduces, the micro-Doppler signatures are more difficult to be recognized from the spectrogram results. The time-varying micro-Doppler signatures are no longer identifiable in Fig. 3(c), whereas in Fig. 3(d), no Doppler signatures can be visually observed.

3.2 Inverse Radon Transform

The IRT utilizes the clear periodicity of the spectrogram because of the rotor rotations. By using a sinusoidal trajectory in the spectrogram domain, the IRT transforms a sinusoidally

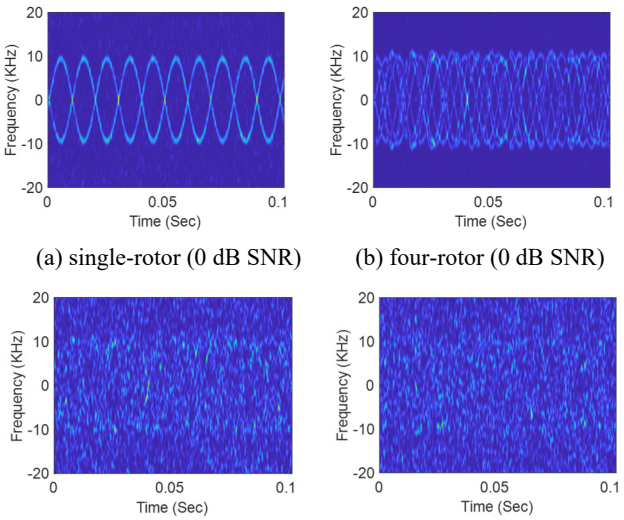

(a) single-rotor (0 dB SNR) (b) four-rotor (0 dB SNR)

(c) four-rotor (−14 dB SNR) (d) four-rotor (−17 dB SNR)

Fig. 3. Spectrogram of drone signals.

varying micro-Doppler signature into a single point in the parameter domain. Note that this is different to conventional Radon transform pairs which are defined over a straight line.

Consider a trajectory model Ω in the spectrogram with instantaneous micro-Doppler frequency defined as:

$$\Omega\colon \hat{f}_{d,k}(t) = -\hat{F}_d \sin\left(j\hat{\omega}_d t + \hat{\phi}_{d,k}(0)\right), \tag{7}$$

which is characterized by maximum micro-Doppler frequency $\hat{F}_d$, rotation radian frequency $\hat{\omega}_d$, and initial phase $\hat{\phi}_{d,k}(0)$. Define the IRT as

$$X(\hat{F}_d, \hat{\omega}_d, \hat{\phi}_{d,k}(0)) = \int_{\Omega} |\mathrm{STFT}(t,f)|^2 d\Omega. \tag{8}$$

Then $X(\hat{F}_d, \hat{\omega}_d, \hat{\phi}_{d,k}(0))$ will render a high value when the parameter set $\{\hat{F}_d, \hat{\omega}_d, \hat{\phi}_{d,k}(0)\}$ matches that of an actual blade defined in Eq. (5).

3.3 Blades of Propellers in a Rotor

In practice, a drone rotor uses two or three propeller blades that are equally separated by 180° or 120°. Utilizing such group structure, we can respectively compute the two-blade and three-blade IRT products as:

$$X_2\left(\hat{F}_d, \hat{\omega}_d, \hat{\phi}_{d,k}(0)\right) = \left[X\left(\hat{F}_d, \hat{\omega}_d, \hat{\phi}_{d,k}(0)\right) \cdot X\left(\hat{F}_d, \hat{\omega}_d, \hat{\phi}_{d,k}(0) + 180^{\circ}\right)\right]^{\frac{1}{2}}, \tag{9}$$

$$X_3\left(\hat{F}_d, \hat{\omega}_d, \hat{\phi}_{d,k}(0)\right) = \left[X(\hat{F}_d, \hat{\omega}_d, \hat{\phi}_{d,k}(0)) \cdot X\left(\hat{F}_d, \hat{\omega}_d, \hat{\phi}_{d,k}(0) + 120^{\circ}\right) X\left(\hat{F}_d, \hat{\omega}_d, \hat{\phi}_{d,k}(0) + 240^{\circ}\right)\right]^{\frac{1}{3}}. \tag{10}$$

Utilizing such group structure increases the detectability against noise and helps identify how many propeller blades are there in each rotor.

Once these parameters are estimated from the peaks in the parameter domain, we can take $\hat{\omega}_d$ and $\hat{\phi}_{d,k}(0)$ as the estimates for ω_d and $\phi_{d,k}(0)$, respectively. In addition, $\hat{F}_d$ is related to $-(2/\lambda)\bar{L}\omega_d \cos(\beta)$ thus can be used to estimate the average blade length projected in the LOS direction, $\bar{L}\cos(\beta)$, given that ω_d is first estimated and λ is known.

4. Simulation Results

For the visualization convenience, the IRT results will be illustrated with respect to the rotation frequency and the initial blade phase, for a specific assumed value of $\bar{L}\cos(\beta)$. Note that $\bar{L}\cos(\beta)$ is suited for this purpose because it is shared by all propeller blades whereas $\hat{F}_d$ may vary with rotors when they have different rotation frequencies.

4.1 Effect of Assumed $\bar{L}\cos(\beta)$ Values

In Fig. 4, we first show IRT results in dB scale with different assumed values of $\bar{L}\cos(\beta)$ for the four-rotor results corresponding to the spectrogram shown in Fig. 3. The input SNR is 0 dB. Fig. 4(a) shows that, when $\bar{L}\cos(\beta)$ is correctly estimated, the IRT results show clearly peaks corresponding to the correct rotation frequency and initial phase. On the other hand, Fig. 4(b) shows that, when the estimated value of $\bar{L}\cos(\beta)$ does not matches the correct one, the peak values are much lower (10% lower value of $\bar{L}\cos(\beta)$ is used in this plot). Note that the same dynamic range is used in the two plots to clearly compare the peak levels. Therefore, correct values of $\bar{L}\cos(\beta)$ can be estimated by seeking the highest peak IRT values. In the subsequent results, correct estimation of $\bar{L}\cos(\beta)$ is assumed.

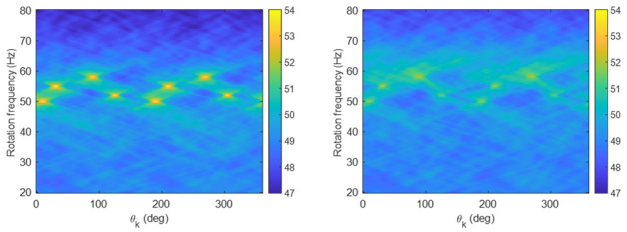

(a) correct $\bar{L}\cos(\beta)$ (b) incorrect $\bar{L}\cos(\beta)$

Fig. 4. IRT results using correct and incorrect (10% lower) assumed values of $\bar{L}\cos(\beta)$. The input SNR is 0 dB.

4.2 IRT and IRT Product for Weak Signals

Fig. 5 shows the IRT and IRT product results for lower input SNR levels of −14 dB and −17 dB. For the −14 dB input SNR case, compared to the spectrogram shown in Fig. 3(a) that cannot identify the micro-Doppler signatures, six peaks can be clearly identified in Fig. 5(a) from such weak signals, while two peak points show lower values. The IRT product shown in Fig. 5(b) provides improved results which enable accurate estimation of parameters of the rotation frequency and blade position phase.

Fig. 5(c) shows the IRT results for the case with −17 dB SNR. The peaks values are still observed, but there are several spurious peaks that make the parameter estimation difficult. In comparison, the IRT product depicted in Fig. 5(d) suppressed such spurious peaks for enhanced identification and parameter estimation.

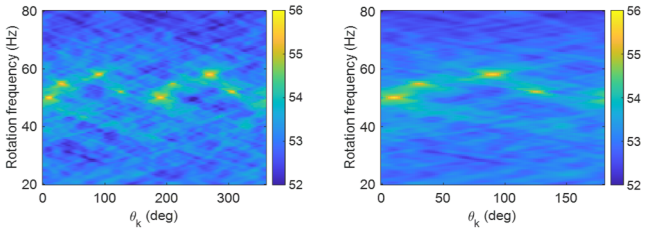

(a) IRT (−14 dB SNR) (b) IRT product (−14 dB SNR)

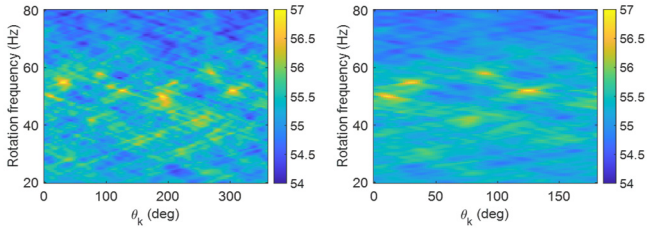

(c) IRT (−17 dB SNR) (d) IRT product (−17 dB SNR)

Fig. 5. IRT and IRT products with different input SNR levels.

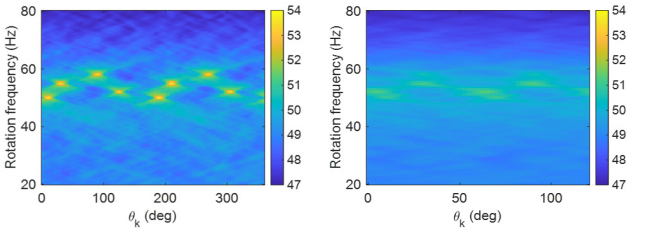

(a) IRT (−10 dB SNR) (b) IRT product (−10 dB SNR)

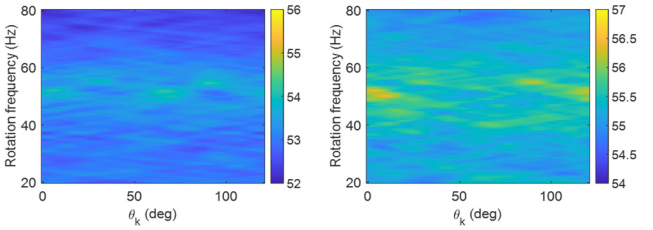

(c) IRT product (−14 dB SNR) (d) IRT product (−17 dB SNR)

Fig. 6. IRT products with incorrect IRT product orders.

4.3 Incorrect IRT Product Order

When the order of IRT product does not match the number of propeller blades in a rotor, the IRT product shows lower peak values, thereby indicating invalid IRT product order.

Fig. 6(a) shows the IRT result for −10 input SNR case, and the corresponding IRT product, in an incorrect order of three, i.e., Eq. (10), is shown in Fig. 6(b). We use the same color scale in both plots. It is observed that, due to the incorrect IRT product order, the IRT product does not provide peaks with comparable peak values. Figs. 6(c) and 6(d) show the IRT products in the same incorrect IRT product order case for input SNR of −14 dB and −17 dB, respectively. The color scale respectively matches their IRT results shown in Figs. 5(a) and 5(c). Again, we observe that no peaks with comparable peak values are observed in these two plots.

4. Conclusion

We have proposed drone Doppler signature analyses based on spectrogram followed by IRT to enable enhanced drone detection and feature extraction. IRT product combining the IRT results obtained for multiple blades in the same rotor further enhances the results for parameter estimation. The proposed analyses account for multiple rotors with different rotation frequencies.

References

[1] B. Li, Z. Fei, and Y. Zhang, "UAV communications for 5G and beyond: Recent advances and future trends," *IEEE Internet of Things J.*, vol. 6, no. 2, pp. 2241-2263, April 2018.

[2] A. Ahmed, S. Zhang, and Y. D. Zhang, "Multi-target motion parameter estimation exploiting collaborative UAV network," in *Proc. IEEE Int. Conf. Acousti., Speech, Signal Process. (ICASSP)*, Brighton, U.K., May 2019, pp. 4459-4463.

[3] A. Huizing, M. Heiligers, B. Dekker, J. de Wit, L. Cifola, and R. Harmanny, "Deep learning for classification of mini-UAVs using micro-Doppler spectrograms in cognitive radar," *IEEE Aerosp. Electron. Syst. Mag.*, vol. 34, no. 11, pp. 46-56, Nov. 2019.

[4] S. Zaugg, G. Saporta, E. Loon, H. Schmaljohann, and F. Liechti, "Automatic identification of bird targets with radar via patterns produced by wing flapping," *J. Royal Soc. Interface*, vol. 5, March 2008.

[5] S. Rahman and D. A. Robertson, "Radar micro-Doppler signatures of drones and birds at K-band and W-band," *Scientific Rep.*, vol. 8, no. 17396, Nov. 2018.

[6] V. C. Chen, *The Micro-Doppler Effect in Radar*. Artech House, 2010.

[7] V. C. Chen, F. Li, S. Ho, and H. Wechsler, "Micro-Doppler effect in radar: Phenomenon, model, and simulation study", *IEEE Trans. Aerosp. Electron. Syst.*, vol. 42, no. 1, pp. 2-21, Jan. 2006.

[8] V. C. Chen and H. Ling, *Time-Frequency Transforms for Radar Imaging and Signal Analysis*. Artech House, 2002.

[9] B. Boashash (ed.), *Time-Frequency Signal Analysis and Processing, Second Edition*. Academic Press, 2016.

[10] H. I. Choi and W. J. Williams, "Improved time-frequency representation of multicomponent signals using exponential kernels," *IEEE Trans. Acoust., Speech, Signal Process.*, vol. 37, no. 6, pp. 862–871, June 1989.

[11] D. L. Jones and R. G. Baraniuk, "An adaptive optimal-kernel time-frequency representation," *IEEE Trans. Signal Process.*, vol. 43, no. 10, pp. 2361–2371, Oct. 1995.

[12] L. Stankovic, S. Stankovic, I. Orovic, and Y. D. Zhang, "Time-frequency analysis of micro-Doppler signals based on compressive sensing," in M. G. Amin (ed.), *Compressive Sensing for Urban Radars*, CRC Press, 2014.

[13] M. G. Amin, B. Jokanovic, Y. D. Zhang, and F. Ahmad, "A sparsity-perspective to quadratic time-frequency distributions," *Digital Signal Processing*, vol. 46, pp. 175-190, Nov. 2015.

[14] L. Stankovic, M. Dakovic, T. Thayaparan and V. Popovic-Bugarin, "Inverse radon transform–based micro-Doppler analysis from a reduced set of observations," *IEEE Trans. Aerosp. Electron. Syst.*, vol. 51, no. 2, pp. 1155-1169, April 2015.

[15] P. Sathe, A. Dyana, K. P. Ray, D. Shashikiran, and A. Venga-darajan, "Helicopter main and tail rotor blade parameter extraction using micro-Doppler," in *Proc. Int. Radar Symp.*, Bonn, Germany, June 2018, pp. 1-10.